Cell Reports, Volume *42*

Supplemental information

VIP interneuron impairment promotes *in vivo* circuit dysfunction and autism-related behaviors in Dravet syndrome

Kevin M. Goff, Sophie R. Liebergall, Evan Jiang, Ala Somarowthu, and Ethan M. Goldberg

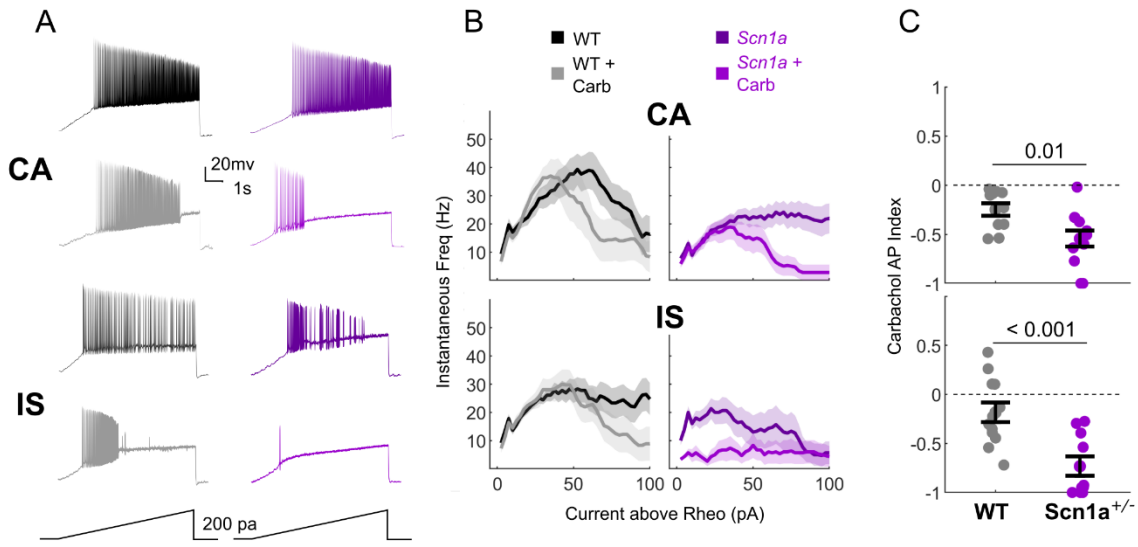

Figure S1: Carbachol has a similar effect on VIP-INs with differing firing patterns.

(A) Example continuous adapting (CA) and irregular spiking (IS) VIP-INs in acute slices from adult *Scn1a*$^{+/-}$ and WT mice. The voltage response to a 200 pA, 8s ramp current at 250 pA/s (as in Figure 1) before and after bath application of 5μm carbachol is shown for each cell.

(B) As in Figure 1B, the average firing frequency response to 8s ramp depolarizations for both cell types and both genotypes.

(C) As in Figure 1E, the effect of carbachol on the total number of spikes generated during an 8s ramp calculated as an index value. Indicated *p*-values represent differences between genotypes.

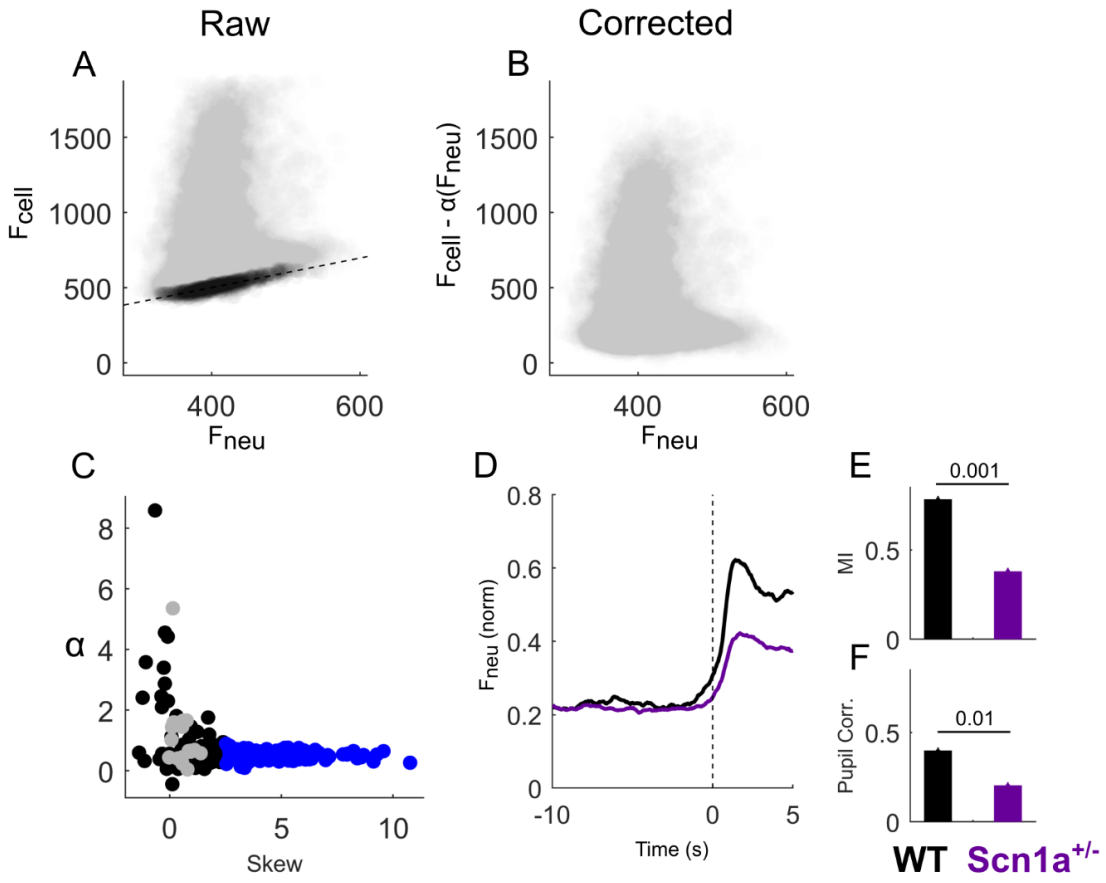

Figure S2: Neuropil background fluorescence correction and reduction in summed neuropil activity of *Scn1a*$^{+/-}$ mice, Related to Figure 1.

(A) Scatterplot of a single non-VIP neuron from a WT mouse with raw cell fluorescence (F_{cell}) plotted on the y-axis, and the background neuropil fluorescence for that cell (F_{neu}) at the corresponding time point. An algorithm to fit the bottom envelope of this plot, corresponding to the lowest F_{cell} for any given value of $F_{neu,}$ was used to calculate the correction factor α (see Methods).

(B) The same as in (A), but now plotting the corrected cellular fluorescence signal $Fcell - \alpha(Fneu)$ on the y axis.

(C) The same process in (A-B) was carried out for all cells in each field of view, including all VIP-INs (*gray*) and non-VIP neurons (*black*). However, to avoid overestimating α for low skew cells, we averaged α for cells with skew >2.5 (*blue*) and used this value for all cells with skew <2.5.

(D) Average normalized neuropil signal (dF_{neu}/F_{0neu}) as in Figure 2E.

(E) Locomotion MI of the neuropil signal was reduced in *Scn1a*$^{+/-}$ mice.

(F) Average correlation coefficient with pupil diameter is also reduced. n = 2511 regions from N = 5 WT mice; n = 4378 regions from N = 6 *Scn1a*$^{+/-}$mice.

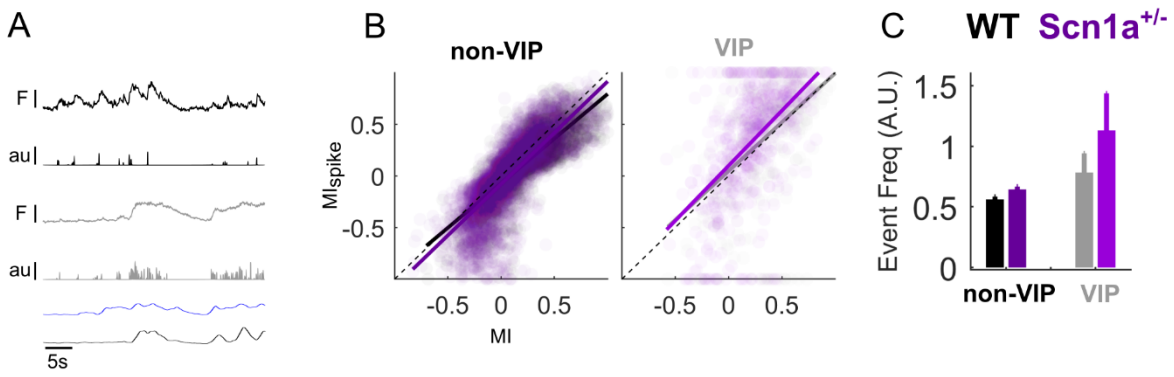

Figure S3: Event deconvolution from dF/F_0 shows no difference in the baseline event frequency at rest, Related to Figure 2.

(A) Example dF/F_0 traces from a WT VIP-IN and non-VIP neuron, with associated z-scored pupil diameter (*blue*) and locomotion (*black*).

(B) Calculating the locomotion MI using either dF/F_0 or deconvolved event trains yields equivalent results. Dots represent values for individual cells, and data is fit with a generalized linear model. Slope + intercept: non-VIP neurons, $0.99x - 0.07$ vs. $0.87x - 0.07$, *Scn1a*$^{+/-}$ vs. WT (p = 0.57, p = 0.72); VIP-INs, $1.07x - 0.1$ vs. $0.95x - 0.05$, *Scn1a*$^{+/-}$ vs. WT (p = 0.33, p = 0.88).

(C) Estimated event rate during stationary epochs is not different between genotypes. n = 2511 tdT- and 368 VIP-INs from N = 5 WT mice, n = 4378 tdT- and 577 VIP-INs from n = 6 *Scn1a*$^{+/-}$ mice.

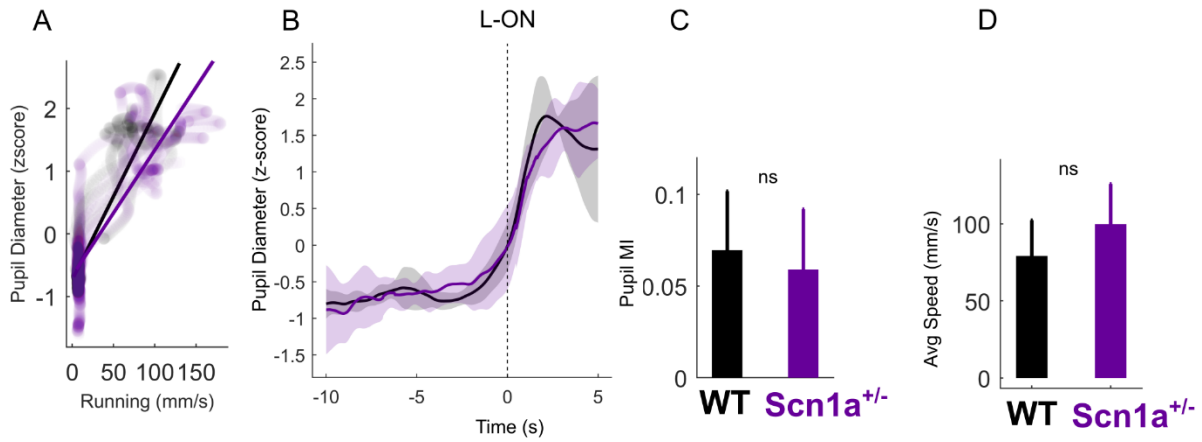

Figure S4: Markers of behavioral state change are consistent across genotypes during 2P imaging sessions, Related to Figure 2.

(A) Scatter plot of pupil diameter and running speed from a single trial from a WT (*gray*) and *Scn1a*$^{+/-}$ mouse (*purple*). Each line represents a simple linear fit to the data.

(B) Average pupil dilation aligned to the onset of locomotion for all WT and *Scn1a*$^{+/-}$ mice.

(C) The increase in pupil diameter during running bouts calculated as an index value.

(D) Average running speed during locomotion bouts of all WT and *Scn1a*$^{+/-}$ mice.

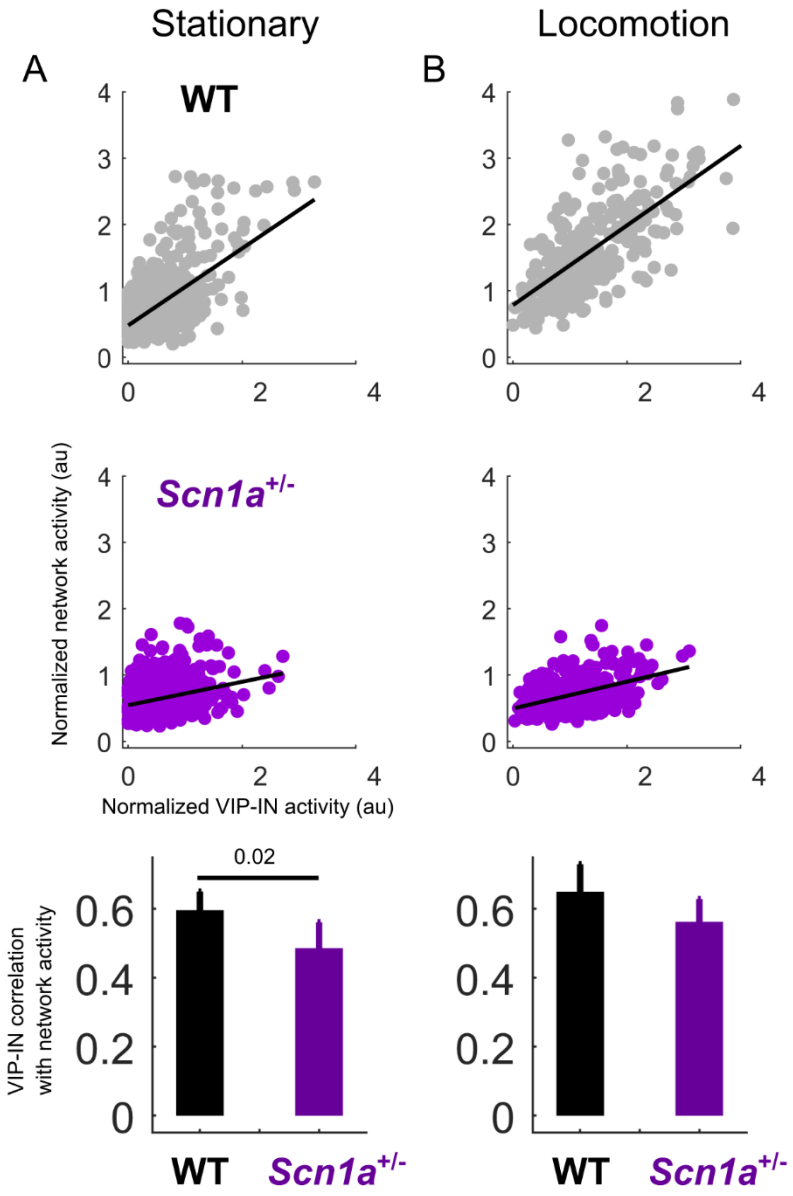

Figure S5: VIP-IN to non-VIP-IN correlation during quiet wakefulness is reduced in *Scn1a*$^{+/-}$ mice, Related to Figure 2.

(A) *Top*: Scatter plot of normalized non-VIP neurons and VIP-IN activity for an example imaging experiment during stationary epochs. Each dot represents activity during a 1 second interval. *Middle*: the same for an example *Scn1a*$^{+/-}$ mouse. *Bottom*: Average VIP-IN to non-VIP correlation is reduced in *Scn1a*$^{+/-}$ mice during stationary epochs (Pearson correlation coefficient, - 0.11 ± 0.04, p = 0.02).

(B) The same as in (A), but during locomotion bouts. Note the increased VIP-IN and non-VIP

activity in the WT mouse that is not present in the *Scn1a*$^{+/-}$ mouse. *Bottom*: *Scn1a*$^{+/-}$ mice trend lower in VIP-IN:network correlation during locomotion bouts (-0.08 ± 0.05, p = 0.1).

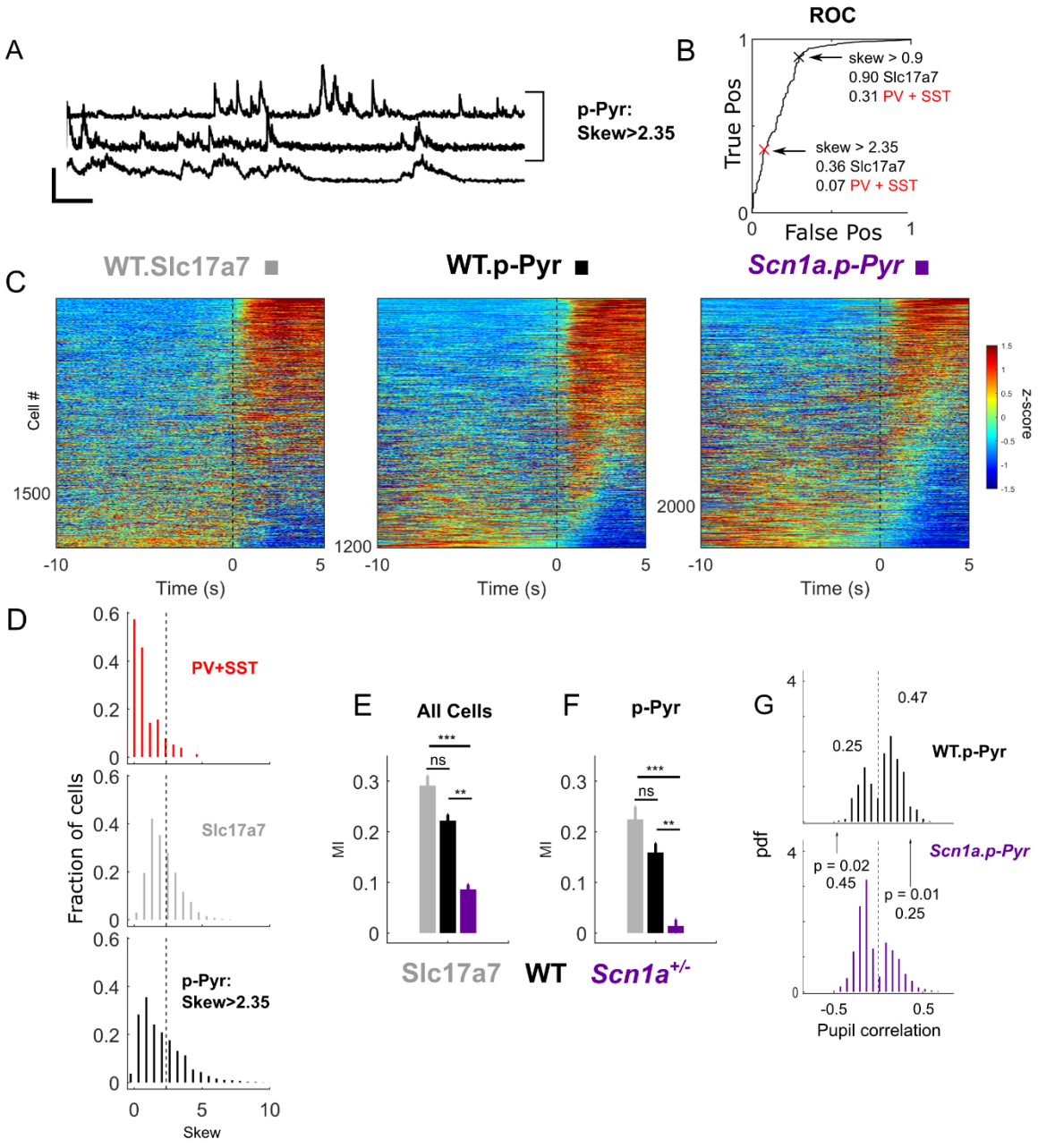

Figure S6: Isolating definitive pyramidal neurons from tdT- non-VIP neurons, Related to Figure 2.

(A) Calcium traces (as shown in Figure 2B) from tdT-negative (tdT-) non-VIP neurons have a range of skew values, where most cells show high skew cells show sharp transients, and some low skew cells have broader transients. Scale:2 zscore (au), 10 seconds.

(B) Receiver operating characteristic (ROC) curves comparing the skew values from pyramidal neurons recorded from WT.Slc17a7-Cre mice to skew values from PV and SST-INs in previously reported data.[1] The optimal value for distinguishing tdT- neurons from PV and SST-INs is

indicated by the black X, and when false positives (IN classified as pyramidal neurons) are weighted 2.5-fold as much as false negative, the optimum value is shown by the red X. We used this more conservative cutoff of 2.35 in our data to isolate a population of non-VIP neurons that are highly likely to be pyramidal neurons (p-Pyr). Estimating ~10% of layer II/III to be other IN subtypes, this cutoff would achieve ~98% purity pyramidal neurons in our tdT$^-$ population.

(C) Heatmap of the z-scored dF/F_0 response from each WT and *Scn1a*$^{+/-}$ p-Pyr aligned to the onset of locomotion shown alongside definitive pyramidal neurons recorded from WT.Slc17a7 mice.

(D) Histogram of skew values from 180 PV-Cre.tdT+ and 27 SST-Cre.tdT+ cells (combined, red) recorded from *N* = 3 WT.PV-Cre and *N* = 2 WT.SST-Cre mice as well as *n* = 2005 pyramidal neurons from N =3 WT.Slc17a7-Cre mice (grey, 2 male, 1 female) and *n* = 2803 tdT$^-$ from *N* = 5 WT.VIP-Cre mice (black, 3 male, 2 female)).

(E) The average locomotion MI for pyramidal neurons from WT.Slc17a7 mice compared to all tdT$^-$ neurons from WT and *Scn1a*$^{+/-}$ mice (as in Figure 2F).

(F) The same as E but only analyzing putative pyramidal neurons (p-Pyr) with skew >2.34.

(G) Histograms of the correlation coefficient between all p-Pyr and pupil diameter. Only cells that are significantly correlated with pupil diameter are plotted, and the percent which are either positively or negatively correlated are indicated above each histogram. *n* = 1,169 p-Pyr from *N* = 5 WT mice (3 male, 2 female); n = 2,334 p-Pyr from *N* = 6 *Scn1a*$^{+/-}$ mice (2 male, 4 female). All differences between genotypes in Figure 2F-I were maintained when limiting analysis to p-Pyr.

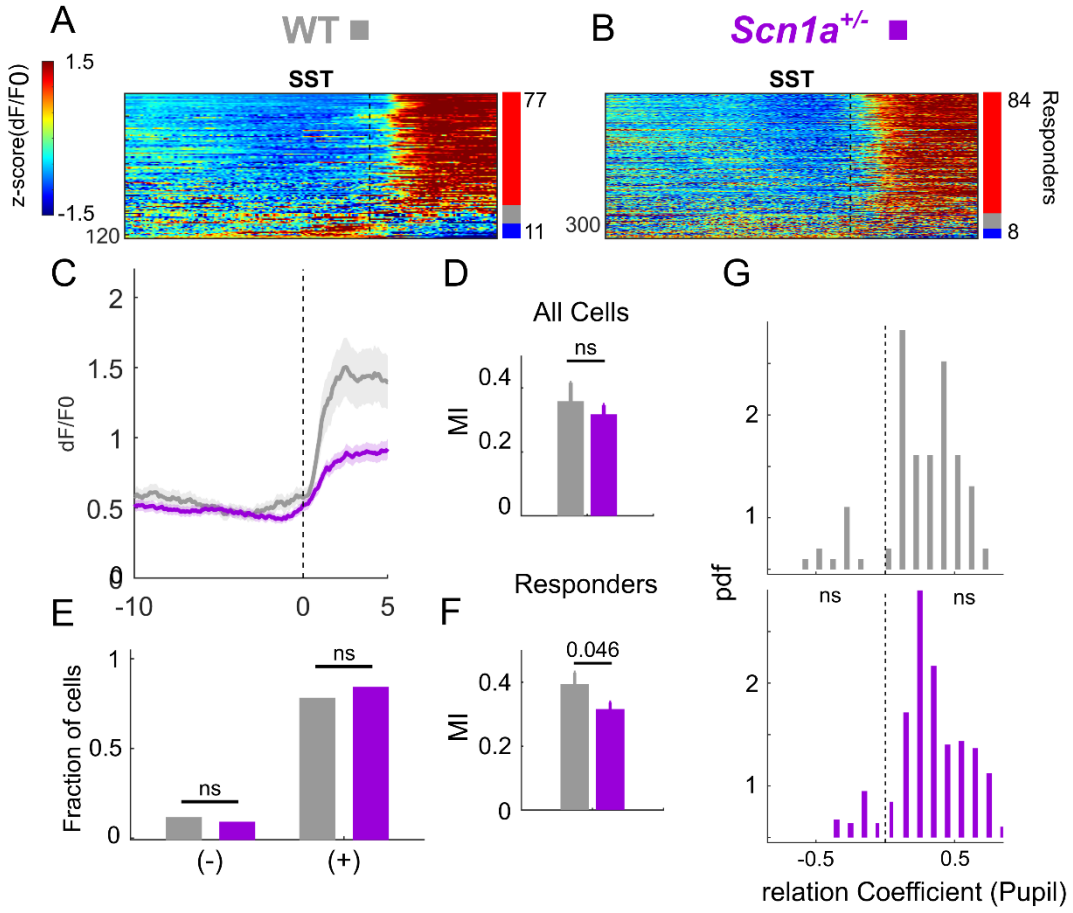

Figure S7: Recruitment of SST-INs during locomotion is maintained in *Scn1a*$^{+/-}$ mice, Related to Figure 2.

(A-B) Heat map showing activity for each cell (as shown in Figure 2C) at the onset of > 5 second locomotion bouts, averaged from multiple running bouts and z-scored within each cell. Bars indicate percentage that are activated (*red* - responder) or inhibited (*blue*) at onset of locomotion.

(C) Average dF/F0 at onset of locomotion across all SST-INs (mean and 95% CI). Black dotted line in (A-C) represents onset of locomotion.

(D) Modulation of dF/F_0 during locomotion measured as an index value calculated for all cells (MI; see Methods).

(E) Fraction of cells activated (+) or inhibited (-) at onset of locomotion as in (B-C) by genotype. Responders were cells that showed significant positive (+) or negative (-) correlation to locomotion vs. shuffled behavioral data. No significant differences across genotype.

(F) MI as in F but for those cells activated during locomotion (Responders) which showed an increase in activity in WT SST-IN responders responsible for the apparent difference in D.

(G) Histograms of the time-zero correlation coefficient between the activity of individual cells versus pupil diameter. There were no significant differences across genotype. *n* = 123 SST-INs from *N* = 4 WT mice (2 male, 2 female); *n* = 335 SST-INs from *N* = 5 *Scn1a*$^{+/-}$mice (3 male, 2 female).

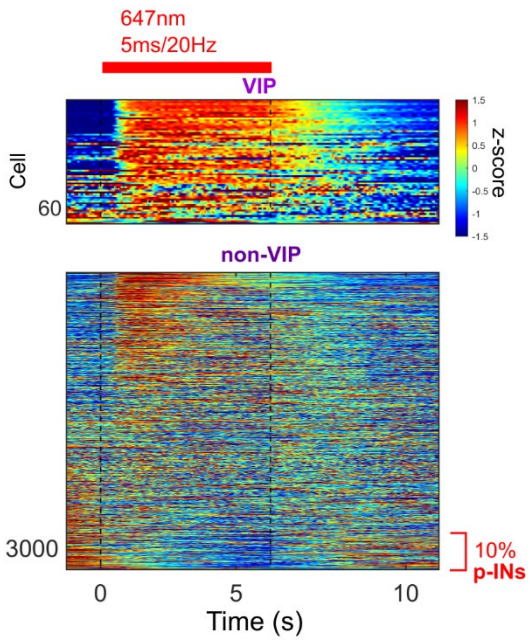

Figure S8: Diverse network responses in response to optogenetic stimulation of VIP-INs, Related to Figure 3.

Heatmap representing z-scored dF/F_0 of cells during 2P imaging experiments aligned to red laser stimulation (described in Figure 3). *Top*: VIP-INs expressing ChrimsonR.tdT are uniformly activated by red light during stationary epochs. *Bottom*: local non-VIP neurons show diverse responses, with a small disinhibitory response in most cells, and a strong inhibitory response in 10% of cells that represent putative inhibitory INs (p-INs) targeted directly by VIP-INs. Cells are arranged based on correlation with laser stimulation, and the bottom 10% (large negative), which approximates the number of non-VIP neurons in layer II/III [2], are taken to be p-INs.

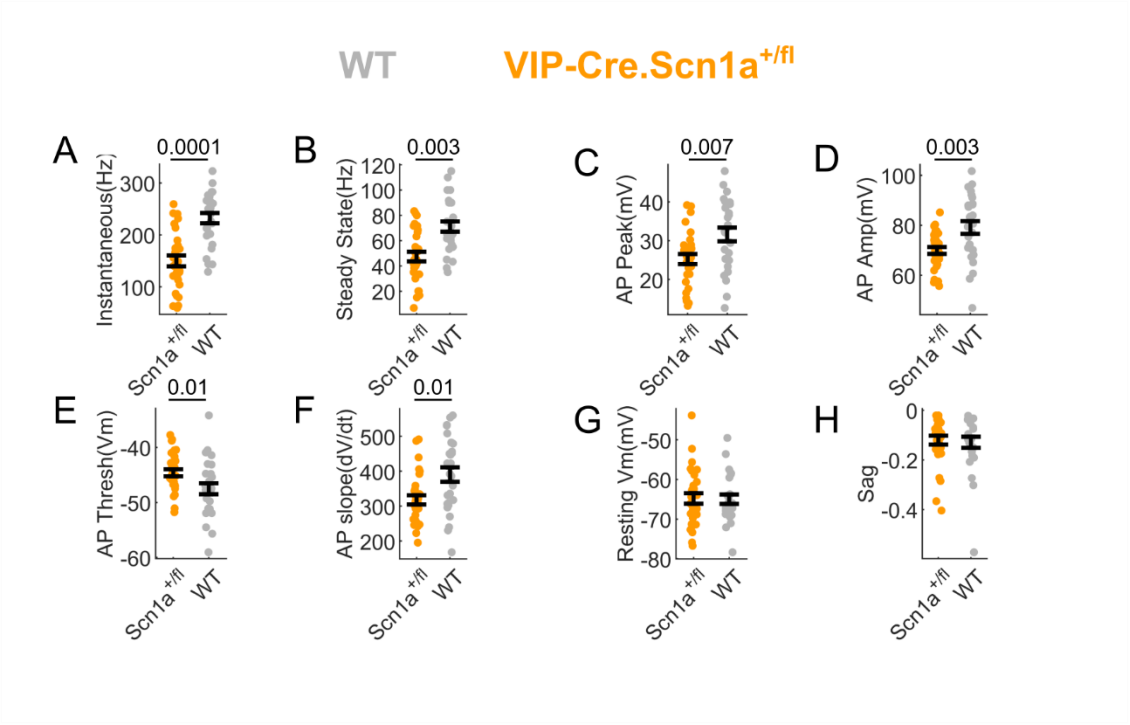

Figure S9. VIP-IN specific loss of *Scn1a* recapitulates the cellular deficits observed in VIP-INs in global *Scn1a*$^{+/-}$ mice, Related to Figure 4.

A-B) Measurements of repetitive firing: (A) Maximum instantaneous firing frequency and (B) maximum steady state firing frequency are reduced in VIP-Cre.*Scn1a*$^{+/fl}$ mice.

(C-F) Several properties of single action potentials including: (C) AP peak voltage; (D) amplitude (Peak – threshold). (E) Action potential voltage threshold; and (F) AP maximum rise slope are impaired in VIP-Cre.*Scn1a*$^{+/fl}$ mice.

(G-H) Other intrinsic properties of VIP-INs which do not directly reflect function of voltage-gated Na^+ channels are unaffected, including: (G) Resting membrane potential and (H) voltage sag in response to a -50 pA square current injection. *n* = 30 VIP-INs from 4 VIP-Cre.*Scn1a*$^{+/fl}$ mice, and *n* = 27 VIP-INs from 4 WT mice. CA and IS VIP-INs were not analyzed separately but IS qualitatively showed the most severe impairment as we have previously reported.[3]

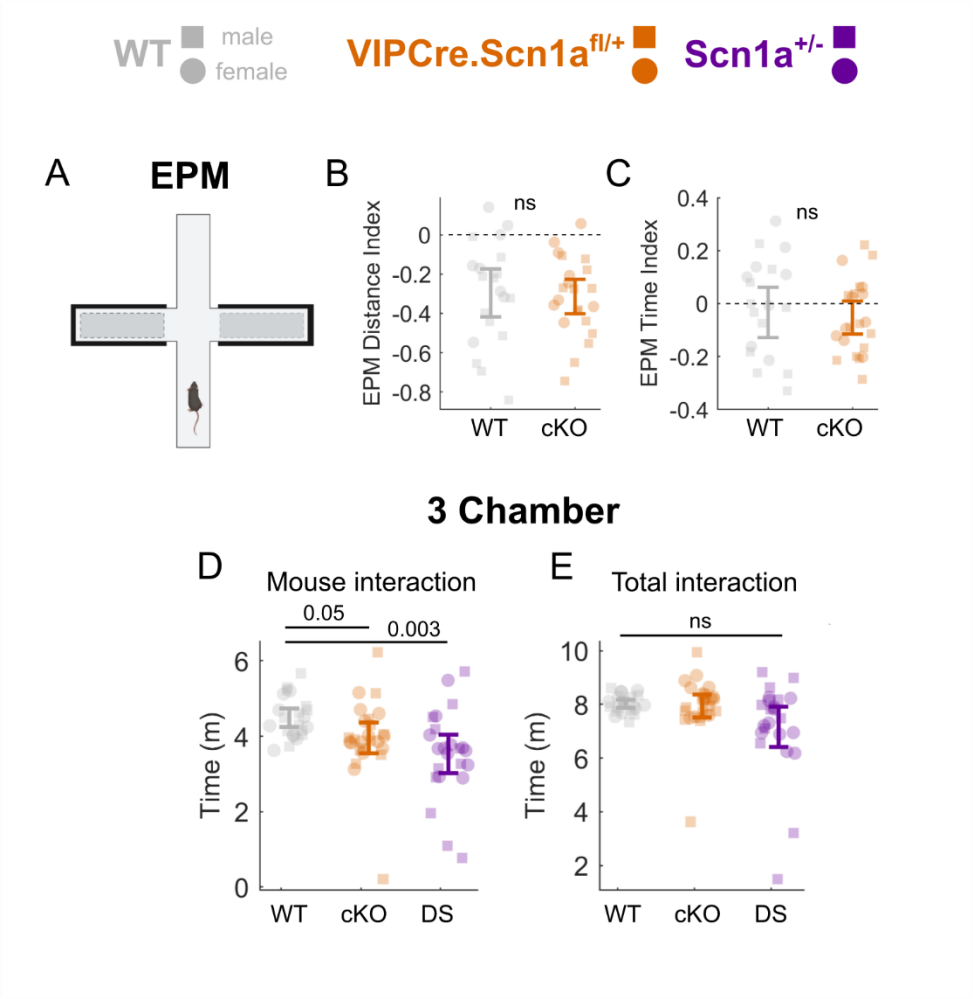

Figure S10: Additional behavioral data for elevated plus maze and three chamber task, Related to Figure 6.

(A) Diagram of the elevated plus maze with two open and two closed arms.

(B) Index of distance traveled in the open arm of the elevated plus maze.

(C) Index of the total time spent exploring the open arm. An index of 0 in B-C (dotted line) indicates equal time/distance in the open/closed arm. *N* = 26 (13 M, 13 F) VIPCre.*Scn1a*$^{fl/+}$ and *N* = 22 (12 M, 10 F) WT mice.

(D) Total time during a 10-minute 3 chamber task spent in the novel mouse chamber (Compare to Figure 6A).

(E) Total time interacting with either the mouse or empty cage during a 10-minute 3 chamber task. No differences between genotypes.

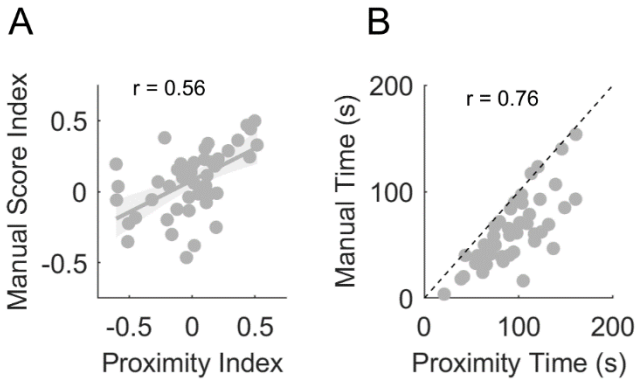

Figure S11: Comparison of DLC based proximity scoring and blinded manual scoring of NOR interactions, Related to Figure 6.

(A) Correlation of the time spent interacting with the novel object as an index, either calculated from manually scored videos or based on proximity from DLC markerless tracking.

(B) The total time spent exploring either the novel or familiar object when scored manually vs with DLC. Blinded manual scoring rarely produces ‘more’ time interacting (above the dotted line) but often produces a lower amount of total interaction, typically by disregarding grooming or freezing epochs when the animal is close to, but not exploring, the object.

Network	Resolution	FPS (Hz)	Mouse parts labelled (connected by a skeleton)	Apparatus labelled
Three Chamber	960x540	30	Nose, neck, tail base, tail tip	Plexiglass dividers, mouse cage, empty cage
Open field/NOR	960x540	30	Nose, neck, tail base, tail tip, paws, ears	Corners of chamber, 4 demarcated positions 3 inches from the wall, objects if present
EPM	1280x720	30	Nose, neck, tail base, tail tip	Entrance to Open and closed arms
Pupillometry	512x440	100	4 points on pupil (top, bottom, left, right), 2 most posterior whiskers (insertion and tip)	N/A

Table S1. Data and network training parameters used in DLC pose estimation.

Supplemental References

1. Somarowthu, A., Goff, K. M. & Goldberg, E. M. Two-photon calcium imaging of seizures in awake, head-fixed mice. *Cell Calcium* **96**, 102380 DOI:https://doi.org/10.1016/j.ceca.2021.102380.

2. Rudy, B., Fishell, G., Lee, S. & Hjerling-Leffler, J. Three groups of interneurons account for nearly 100% of neocortical GABAergic neurons. *Dev. Neurobiol.* **71**, 45–61 DOI:10.1002/dneu.20853.

3. Goff, K. M. & Goldberg, E. M. Vasoactive intestinal peptide-expressing interneurons are impaired in a mouse model of dravet syndrome. *Elife* **8**, 1–28 DOI:10.7554/eLife.46846.